Optical isolation of circularly polarized light with a spontaneous magnetoelectric effect

Filipa R. Prudêncio[1,*] and Mário G. Silveirinha[1,2,†]

[1]*Department of Electrical and Computer Engineering, Instituto de Telecomunicações, Instituto Superior Técnico, University of Lisbon, Avenida Rovisco Pais, 1, 1049-001 Lisboa, Portugal*

[2]*Department of Electrical Engineering, Instituto de Telecomunicações, University of Coimbra, 3030 Coimbra Portugal*

(Received 19 January 2016; published 25 April 2016)

The optical isolation functionality is of key importance in many photonic systems. However, a robust optical isolation is rather challenging to obtain due to the weak nonreciprocal response of conventional materials. Here, we theoretically explore novel solutions to obtain one-way propagation of circularly polarized light using materials with a spontaneous nonreciprocal response combined with chiral metamaterials. Furthermore, we investigate the opportunity of using standard anisotropic nonreciprocal materials (e.g., ferrites or bismuth iron garnet) to obtain the optical isolation of circularly polarized light.

I. INTRODUCTION

Optical isolators are ubiquitous in microwave and optical systems and are vital to protect a light source from undesired backreflections which could disturb its normal operation [1]. It is well known that asymmetric light flows imply a broken time-reversal symmetry. Usually, this is achieved with the help of a biasing magnetic field that provides the nonreciprocal response [2–8]. Indeed, a Faraday rotator is the crucial element of conventional optical isolators. At optical communication wavelengths, a Faraday rotator is usually implemented with iron garnets and related materials [9–11]. However, there are several drawbacks inherent to the use of static magnetic fields in terms of size, weight, and temperature sensitivity, which are incompatible with on-chip miniaturization of all-optical circuits. Thus, there is currently a great interest in the development of alternative compact devices that can provide for the "one-way" propagation functionality in future integrated photonic platforms [12–19]. Interestingly, it has been recently shown that the effect of a static magnetic field can be mimicked with the help of active components (transistors) at microwave frequencies [20,21]. Such a paradigm circumvents many of the restrictions of permanent magnets and relies on nonreciprocal gyrotropic metasurfaces. Other less conventional approaches that also enable a nonreciprocal response explore nonlinear effects [22], a temporal refractive-index modulation [23], or moving media [24]. Also, recently there has been a great interest in the application of topological methods to the design of photonic devices with unidirectional characteristics [25–31].

Importantly, some materials directly available in nature can have a *spontaneous* nonreciprocal magnetoelectric response, which does not require any type of biasing, being the most well-known example chromium oxide (Cr_2O_3) [32]. It was also theoretically predicted that some crystalline structures with a magnetic order may be characterized by an isotropic linear spontaneous nonreciprocal magnetoelectric coupling [33], even though the strength of the magnetoelectric effect is generally weak. In parallel with these developments, a new phase of matter known as topological insulators was discovered some

years ago [34,35]. One of the exotic properties of *electronic* topological insulators is that they may be characterized by a topological magnetoelectric effect modeled by Tellegen-type constitutive relations [36–42] such that an electric excitation generates a nonreciprocal isotropic magnetic response and vice versa. The use of these materials in the context of photonics is relatively unexplored, and since they do not require external biasing elements, one may envision that they can play a role in future photonics platforms for optical isolation.

Inspired by these developments, here we investigate novel planar designs for the one-way propagation of circularly polarized light relying on the combination of a chiral metamaterial and a nonreciprocal element. It is shown that by combining these two building blocks it may be possible to have in ideal conditions a nearly perfect optical isolation of two propagation channels. Furthermore, we outline different configurations for the nonreciprocal element, relying either on media with a spontaneous (Tellegen-type) nonreciprocal response (e.g., antiferromagnet electronic topological insulators [34]) or alternatively relying on conventional nonreciprocal materials (ferrites or iron garnets).

This article is organized as follows. In Sec. II we briefly describe the general idea and working principles of the proposed optical isolator for circular polarized light formed by a chiral metamaterial and a nonreciprocal element. The design of the chiral metamaterial element and the conditions under which it can have a highly asymmetric transmissivity strongly dependent on the light helicity are discussed in Sec. III. Similarly, in Sec. IV we outline different solutions for the nonreciprocal element relying either on conventional magneto-optic materials or on media with a spontaneous nonreciprocal response. In Sec. V, it is verified that by combining the individual responses of the nonreciprocal element and of the chiral metamaterial it is possible to have a one-way energy flow and a nearly perfect optical isolation. Finally, in Sec. VI the main conclusions are drawn. In this article, the time variation of the electromagnetic fields is assumed to be of the form $e^{-i\omega t}$.

II. OPTICAL ISOLATOR FOR CIRCULARLY POLARIZED LIGHT

Here, we describe the general idea to realize an optical isolator for circularly polarized light. Figure 1(a) illustrates

---

*Corresponding author: filipa.prudencio@lx.it.pt
†mario.silveirinha@co.it.pt
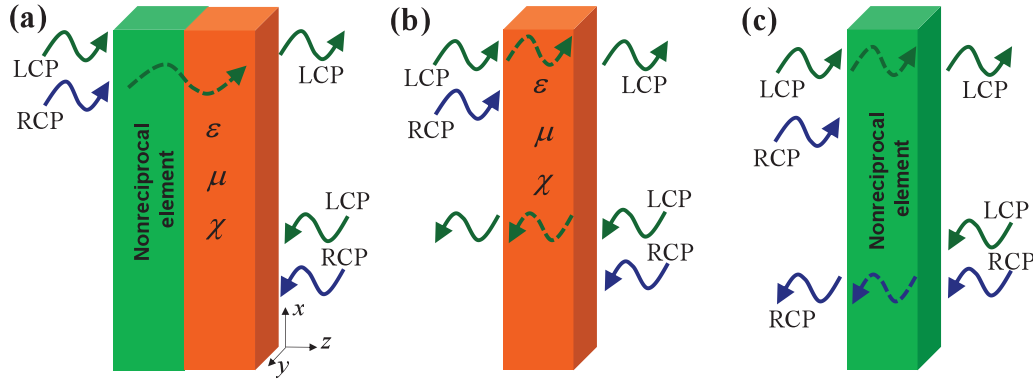
FIG. 1. Optical isolation with a chiral metamaterial and a nonreciprocal element. Pairs of arrows with the same color represent an incident wave and the corresponding transmitted wave. Unpaired arrows represent incident waves that are blocked by the material structure. (a) Combined response of the two elements. The only wave that is not blocked by the structure is an LCP wave propagating from the left to the right. (b) Asymmetric light transmission by a suitably designed chiral slab; the LCP wave goes through the chiral slab, and the RCP wave is blocked. (c) Asymmetric light transmission by a suitably designed nonreciprocal element; for incidence from the left to the right (the right to the left) only the LCP (RCP) wave goes through the nonreciprocal element.

the generic geometry of the proposed isolator. It is formed by two juxtaposed building blocks with tailored material responses. One of the building blocks is a chiral metamaterial, and the second building block is a nonreciprocal element. In the following, we explain the operation of the two elements.

Chiral media are a special class of materials with magnetoelectric coupling determined by the handedness of the structural unities [38]. Among other applications, these materials can be used to obtain polarization rotation (optical activity) and polarization conversion [38,43]. The photonic modes in an unbounded chiral medium are right circular polarized (RCP) waves or left circular polarized (LCP) waves and have distinct propagation properties. Previous works have shown that it is possible to design a chiral metamaterial slab that blocks a certain circularly polarized wave (let us say a RCP wave) and lets an excitation with the opposite helicity (LCP wave) through [44–49] [Fig. 1(b)]. As detailed below, our solution explores this asymmetric response of chiral metamaterials to circularly polarized waves with different helicities.

On the other hand, the nonreciprocal element may also be designed to have similar properties (blocks RCP waves and lets LCP waves through) when the incoming wave propagates along a specific space direction [let us say from the left to the right (L-R), Fig. 1(c)]. This will be demonstrated in Sec. IV. However, because the electromagnetic response of the usual magneto-optical materials is not invariant under a space inversion, when the incoming wave propagates in the opposite direction [from the right to the left (R-L), Fig. 1(c)] the responses to LCP and RCP waves are interchanged. Thus, when the chiral material slab is combined with the nonreciprocal element only a LCP wave propagating from the left to the right can pass through the system [Fig. 1(a)]. Therefore, the proposed configuration provides the optical isolation functionality and operates with circularly polarized light. In the following sections, we explore different solutions to implement each of the basic elements of the

proposed isolator and provide a detailed analysis of its performance.

III. THE CHIRAL METAMATERIAL

Next, we analyze under which conditions a chiral metamaterial slab may have a strongly asymmetric response to circularly polarized waves with different helicities. To this end, first the chiral slab is modeled as a continuous medium [Fig. 1(b)] with constitutive relations $\mathbf{D} = \varepsilon_0 \varepsilon \mathbf{E} + c^{-1} i \chi \mathbf{H}$ and $\mathbf{B} = \mu_0 \mu \mathbf{H} - c^{-1} i \chi \mathbf{E}$, where ε_0 and μ_0 are the vacuum permittivity and permeability, respectively, $c = 1/\sqrt{\varepsilon_0 \mu_0}$ is the speed of light in the vacuum, ε is the relative permittivity, μ is the relative permeability, and χ is the chirality parameter. It is assumed that the dimensionless material parameters satisfy the Condon dispersion model [50],

$$\varepsilon(\omega) = \varepsilon_c + \Omega_\varepsilon \omega_R^2 / (\omega_R^2 - \omega^2 - i\gamma\omega),$$
$$\mu(\omega) = \mu_c + \Omega_\mu \omega^2 / (\omega_R^2 - \omega^2 - i\gamma\omega), \quad (1)$$
$$\chi(\omega) = \Omega_\chi \omega_R \omega / (\omega_R^2 - \omega^2 - i\gamma\omega),$$

where ω_R is the resonance frequency, γ is a damping frequency, and Ω_ε, Ω_μ, and Ω_χ determine the resonance strength. The transmission and reflection coefficients for circularly polarized waves that impinge on a chiral slab with thickness d are as follows [38,50]:

$$T_\pm^L = \frac{4z e^{ik_\pm d}}{(1+z)^2 - (1-z)^2 e^{2ink_0 d}},$$
$$R \equiv R_\pm = \frac{(1-z^2)(e^{2ink_0 d} - 1)}{(1+z)^2 - (1-z)^2 e^{2ink_0 d}}. \quad (2)$$

In the above, $k_\pm = k_0(n \pm \chi)$, $k_0 = \omega/c$, $n = \sqrt{\mu\varepsilon}$, and $z = \mu/n = \sqrt{\mu/\varepsilon}$ is the normalized impedance. The subscript $\pm$ determines the relevant electric-field distribution $\mathbf{E} = E(z)\mathbf{e}_\pm$, where $E(z)$ is some function of z and $\mathbf{e}_+ = \hat{\mathbf{x}} + i\hat{\mathbf{y}}$ and $\mathbf{e}_- = \hat{\mathbf{x}} - i\hat{\mathbf{y}}$ with z being the direction of stratification [see Fig. 1(b)]. In the case where the incidence is from

the L-R (propagation along the positive z direction) the eigenvectors $\mathbf{e}_+$ and $\mathbf{e}_-$ are associated with RCP and LCP waves, respectively. On the other hand, for an incoming wave propagating from the R-L (propagation along the negative z direction), the eigenvectors $\mathbf{e}_+$ and $\mathbf{e}_-$ are associated with LCP and RCP waves. The transmission coefficient for incident RCP waves is $T^{\mathrm{RCP}} = T^L_+$ and for incident LCP waves is $T^{\mathrm{LCP}} = T^L_-$, independent if the incoming wave propagates in the direction L-R or R-L [38]. The reflection coefficient R is independent of the polarization state. Interestingly, even though the chiral medium is a reciprocal material, it is possible to have asymmetric transmissions for waves with different helicities, i.e., $|T^{\mathrm{LCP}}| \neq |T^{\mathrm{RCP}}|$ when the chiral material is lossy [44,50].

Following Ref. [39], to have a physically realizable material response the parameters Ω_ε, Ω_μ, and Ω_χ must satisfy the conditions $\Omega_\varepsilon \Omega_\mu - \Omega_\chi^2 > 0$ with $\Omega_\varepsilon > 0$. The regime of strongly asymmetric transmissions occurs when Ω_χ is near $\pm\sqrt{\Omega_\varepsilon \Omega_\mu}$ and the damping parameter is nonzero $\gamma > 0$. For example, if $\varepsilon_c = \mu_c$ it may be checked that at $\omega = \omega_{R0} \equiv \omega_R \sqrt{\Omega_\varepsilon/\Omega_\mu}$ one has $z = 1$ so that $R = 0$ and $T^L_\pm = e^{ik_\pm d}$. In these conditions in the limit $\Omega_\chi = s\sqrt{\Omega_\varepsilon \Omega_\mu}$ (with $s = \pm$) one of the circularly polarized waves is perfectly transmitted through the chiral slab $|T^L_{-s}| = 1$, whereas the wave with opposite helicity can be strongly attenuated $|T^L_s| = e^{-2(\omega/c)d\,\mathrm{Im}(\varepsilon)}$ for $\omega = \omega_{R0}$ and a sufficiently thick slab. This property is illustrated in Fig. 2(a) for the case of $\varepsilon_c = \mu_c = 1$, $\gamma = 0.1\omega_R$, $\Omega_\varepsilon = 1$, $\Omega_\mu = 0.9$, $\Omega_\chi = +\sqrt{\Omega_\varepsilon \Omega_\mu}$, and for different values of d. As seen, for increasing d we get closer and closer to the regime wherein $|T^{\mathrm{LCP}}| = 1$ and $|T^{\mathrm{RCP}}| \approx 0$.

As is well known, the regime of strongly asymmetric transmission can be mimicked using metamaterials [44,49]. Figure 2(b) depicts the transmission coefficients calculated with CST MICROWAVE STUDIO [51] for a particular metamaterial design at optical frequencies based on conjugated gammadion particles. The structure considered here is the same as in Ref. [44], except that the thickness of the silicon layers was optimized to $d_s = 65$ nm to have an extremely asymmetric response. As seen, at 188.5 THz (which corresponds to a wavelength near 1.55 μm) only the LCP waves can go through the lossy metamaterial slab, whereas the RCP waves are completely blocked independent of the direction from which the slab is illuminated.

IV. THE NONRECIPROCAL ELEMENT

As shown in the previous section, chiral metamaterials enable strongly asymmetric transmissions of circularly polarized waves with opposite helicities, independent of the direction of propagation of the incoming light. In order to implement the optical isolation functionality (Fig. 1), one also needs an element with a transmission response that depends on the direction of propagation of the incident wave, i.e., that is sensitive to whether the incoming wave propagates from the left to the right or from the right to the left. In the following, we discuss different solutions to achieve this.

A. Spontaneous magnetoelectric effect

As mentioned in Sec. I, following the discovery electronic topological insulators, there is a great interest in media
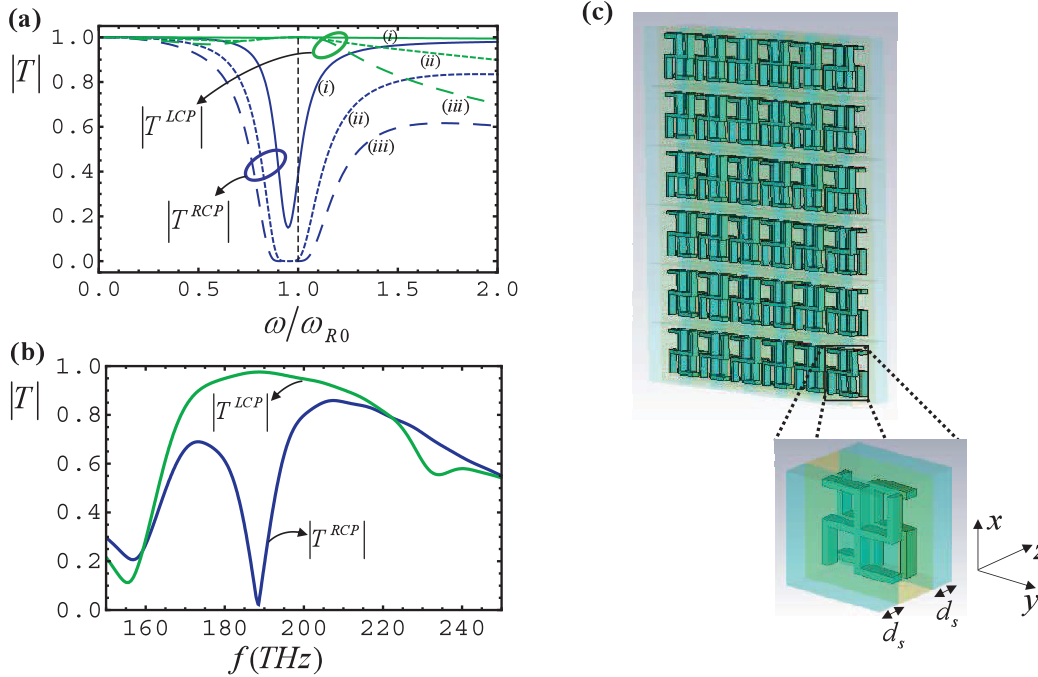
FIG. 2. Strongly asymmetric transmission of circularly polarized light with a lossy chiral metamaterial. (a) $|T^{\mathrm{LCP}}|$ and $|T^{\mathrm{RCP}}|$ as a function of the normalized frequency for a continuous chiral material slab with thickness d and characterized by the Condon dispersive model [Eq. (1)]. The oscillation frequency is normalized to $\omega_{R0} = \omega_R \sqrt{\Omega_\varepsilon/\Omega_\mu}$. (i) $\omega_R d/c = 0.1$, (ii) $\omega_R d/c = 0.5$, and (iii) $\omega_R d/c = 1$. (b) $|T^{\mathrm{LCP}}|$ and $|T^{\mathrm{RCP}}|$ for a planar chiral optical metamaterial formed by a periodic array of conjugated gammadion particles. (c) Geometry of the metamaterial array. The structural parameters are similar to Ref. [44], but the silicon layer thickness was optimized to $d_s = 65$ nm.

with an isotropic nonreciprocal response [33–37]. It has been predicted that topological insulators may be characterized by a topological magnetoelectric effect such that $\mathbf{D} = \varepsilon_0 \varepsilon' \mathbf{E} - \alpha \frac{\theta}{\pi} \frac{1}{\eta_0} \mathbf{B}$ and $\mathbf{H} = \mu_0^{-1} \mu^{-1} \mathbf{B} + \alpha \frac{\theta}{\pi} \frac{1}{\eta_0} \mathbf{E}$ [40,41], where $\alpha = e^2/(2hc\varepsilon_0) \approx 1/137$ is the fine-structure constant, η_0 is the vacuum impedance, and $\theta = \pi(1 + 2n)$ with the n integer is the quantized topological (static) magnetoelectric polarizability. In strong topological insulators the observation of a nonzero value of θ (which has not been achieved yet) seems to require a time-reversal breaking perturbation on the surface of the material, e.g., using an external magnetic field [40]. Interestingly, it has been suggested that in antiferromagnetic topological insulators the quantized magnetoelectric nonreciprocal response may occur spontaneously [34]. It has also been suggested that other antiferromagnetic materials, such as modified pyrochlore compounds may be characterized by a purely isotropic magnetoelectric coupling [33]. The mechanism that provides the magnetoelectric response in these materials is different than in topological insulators, and hence θ is not required to be quantized in the static limit. For example, the density-functional theory calculations of Ref. [33] predict a θ on the order of 0.1–0.2 for pyrochlore compounds. Such a value of θ is comparable with what is found in natural materials, such as Cr_2O_3 which provide an analogous (but anisotropic uniaxial) spontaneous magnetoelectric coupling [33,52].

Next, we assess the opportunity of designing the non-reciprocal element of the optical isolator relying on media with a spontaneous nonreciprocal isotropic magnetoelectric coupling. To begin with, we note that the constitutive relations of such materials can be recast in the Tellegen form [38,42]

$$\mathbf{D} = \varepsilon_0 \varepsilon \, \mathbf{E} + c^{-1} \kappa \mathbf{H}, \quad \mathbf{B} = \mu_0 \mu \, \mathbf{H} + c^{-1} \kappa \mathbf{E}, \quad (3)$$

where κ is the Tellegen parameter, which can be written in terms of θ as $\kappa = -\alpha \frac{\theta}{\pi} \mu$ and $\varepsilon = \varepsilon' + (\alpha \frac{\theta}{\pi})^2 \mu$. Because $\alpha \ll 1$, typically one can safely use the approximation $\varepsilon \approx \varepsilon'$. Because the Tellegen parameter is usually small, we investigate the possibility of enhancing the nonreciprocal effects using a truncated photonic crystal [Fig. 3(a)]. One of the authors has shown in a previous work [42] that the eigenstates of the associated scattering problem are $\mathbf{e}_+ = \hat{\mathbf{x}} + i\hat{\mathbf{y}}$ and $\mathbf{e}_- = \hat{\mathbf{x}} - i\hat{\mathbf{y}}$ (i.e., circularly polarized waves) such that for a normally incident electric field proportional to $\mathbf{e}_\pm$ the reflected field is $R_\pm \mathbf{e}_\pm$ and the transmitted field is $T_\pm \mathbf{e}_\pm$ with R and T being reflection and transmission coefficients, respectively. Importantly, it was demonstrated in Ref. [42] that for arbitrary layered structures formed by Tellegen material slabs the transmission coefficients $T_\pm$ are independent of the direction of arrival of the incoming wave [42],

$$T_+^L = T_+^R \equiv T_+, \quad T_-^L = T_-^R \equiv T_-. \quad (4)$$

In the above the superscript L or R indicates whether the incoming wave comes from the left-hand side or the right-hand side of the structure, respectively. Thus, the transmission coefficients for LCP and RCP waves are related as follows:

$$T_{\mathrm{RCP}}^L = T_{\mathrm{LCP}}^R \equiv T_+, \quad T_{\mathrm{LCP}}^L = T_{\mathrm{RCP}}^R \equiv T_-. \quad (5)$$
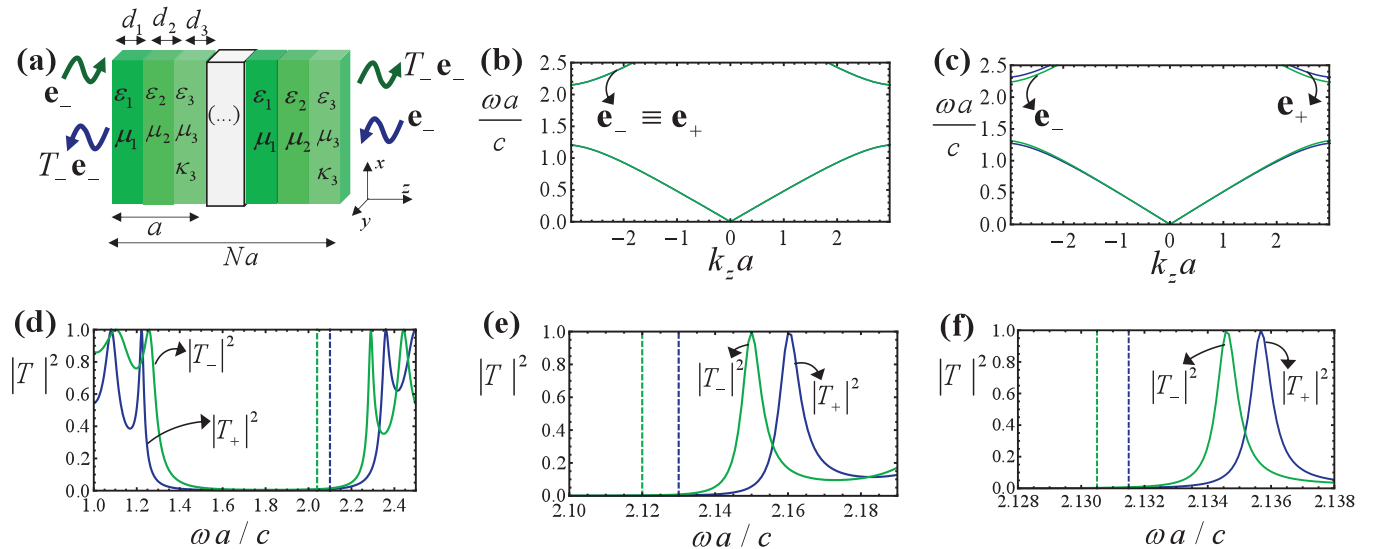
FIG. 3. Nonreciprocal element relying on a spontaneous magnetoelectric effect. (a) Truncated photonic crystal with a unit cell formed by two conventional dielectrics and a Tellegen slab. The photonic crystal is designed so that only incoming waves associated with eigenstate $\mathbf{e}_-$ can be transmitted through the structure. Ideally, for L-R (R-L) incidence the transmitted wave is a LCP (RCP) wave. (b) Band diagram for a Tellegen photonic crystal with a unit cell formed by a dielectric slab ($d_2 = 0.3a$) and a Tellegen slab ($d_3 = 0.7a$) with $\kappa_3 = 69\alpha$. (c) Band diagram for a Tellegen photonic crystal with a unit cell formed by an air layer ($d_1 = 0.06a$), a dielectric slab ($d_2 = 0.24a$), and a Tellegen slab ($d_3 = 0.7a$) with $\kappa_3 = 69\alpha$. (d)–(f) Transmissivities $|T_+|^2$ and $|T_-|^2$ as a function of the normalized frequency for a truncated photonic crystal with a unit cell similar to that of the example (c) with (d) $N = 7$ cells and $\kappa_3 = 69\alpha$, (e) $N = 12$ cells and $\kappa_3 = 10\alpha$, and (f) $N = 25$ cells and $\kappa_3 = \alpha$. In all the examples the dielectric material has parameters ($\varepsilon_2 = 10, \mu_2 = 1$), and the Tellegen material has parameters ($\varepsilon_3 = 2$ and $\mu_3 = 1, \kappa_3$). In panels (d)–(f) the green (blue) dashed vertical lines determine the upper band-gap edge of the modes associated with the polarization $\mathbf{e}_-$ ($\mathbf{e}_+$).

In simple words, the transmission coefficient for LCP (RCP) incident waves propagating from the left to the right is identical to the transmission coefficient for RCP (LCP) incident waves propagating from the right to the left. This type of response is totally different from that of chiral media for which $T_{\mathrm{RCP}}^L = T_{\mathrm{RCP}}^R$ and $T_{\mathrm{LCP}}^L = T_{\mathrm{LCP}}^R$. Hence, to have an optical isolator based on the mechanism outlined in Fig. 1(a), one needs to design the nonreciprocal element in such a manner that one of the transmission coefficients (let us say T_+) is nearly zero while the other transmission coefficient (T_-) has ideally unity amplitude.

As a starting point, we note that a single Tellegen slab cannot provide the desired asymmetric scattering. Indeed, because the material response is isotropic it turns out that for a single Tellegen slab $T_+ = T_-$ [42]. Similarly, a truncated photonic crystal with a unit cell formed by only two different materials is not suitable. The reason is that such a photonic crystal is invariant under twofold (180°) rotation about the x axis, and hence if the truncated structure preserves this symmetry then $T_+ = T_-$ [42]. Indeed, as illustrated in Fig. 3(b), Tellegen photonic crystals formed by only two materials lead to degenerate photonic bands such that the dispersions of the modes with an electric field of the form $\mathbf{E} = E(z)\mathbf{e}_\pm$ are identical: $\omega_+(k_z) = \omega_-(k_z)$. The band diagram of the photonic crystal is calculated as explained in Ref. [42]. Thus, to have a strongly asymmetric transmission with $T_+ \neq T_-$ it is necessary to consider photonic crystals with a unit cell formed by three different materials. Here, we suppose that two of these materials are conventional dielectrics and that the third material has a Tellegen-type response (e.g., an electronic topological insulator) [see Fig. 3(a)].

In the first example, it is supposed that one of the dielectrics is air ($\varepsilon_1 = 1$ and $\mu_1 = 1$) and that the other dielectric is characterized by the parameters $\varepsilon_2 = 10$ and $\mu_2 = 1$; silicon has a similar material response at optical frequencies. The Tellegen material is modeled by the material parameters $\varepsilon_3 = 2$, $\mu_3 = 1$, and $\kappa_3 = 69\alpha$. The thicknesses of the layers are $d_1 = 0.06a$, $d_2 = 0.24a$, and $d_3 = 0.7a$, where a is the lattice constant. Remarkably, in contrast with the example of Fig. 3(b), the band diagram of Fig. 3(c) confirms that for a unit cell with three different materials the eigenstates $\mathbf{e}_\pm$ are no longer degenerate and $\omega_+(k_z) \neq \omega_-(k_z)$ [42]. The difference between the bands $\omega_\pm(k_z)$ is modest on the scale of Fig. 3(c) because the magnetoelectric effect parameter is relatively small. In particular, around the normalized frequency of $\omega a/c \approx 2.25$ (upper band-gap edge) only waves associated with the eigenstate $\mathbf{e}_-$ can propagate through the structure. The transmissivities, $|T_+|^2$ and $|T_-|^2$ are plotted in Fig. 3(d) as a function of the normalized frequency for a truncated photonic crystal with $N = 7$ cells. The transmission coefficients are calculated by matching the tangential $\mathbf{E}$ and $\mathbf{H}$ fields at the interfaces of the different materials as detailed in Ref. [42]. Consistent with the band diagram of Fig. 3(c), a highly asymmetric transmission is obtained at the normalized frequency of $\omega a/c \approx 2.29$, wherein the transmissivity $|T_+|^2$ practically vanishes and $|T_-|^2$ is near unity. Thus, at this oscillation frequency, only incident LCP waves propagating in the L-R direction and incident RCP waves propagating in the R-L direction can be transmitted through this nonreciprocal truncated photonic crystal.

In the previous example, the Tellegen parameter satisfies $\kappa = 69\alpha$, which even though relatively small may still be out of reach with realistic materials. The impact of having a smaller value for κ is that the dispersion of the eigenmodes $\mathbf{e}_\pm$ in Fig. 3(c) becomes more and more similar, and consequently the spectral range wherein $|T_+|^2$ and $|T_-|^2$ may differ appreciably from one another has a smaller bandwidth. In addition, to have comparable asymmetries one needs to consider thicker structures to compensate for the poorer discrimination between the eigenmodes dispersion. These properties are illustrated in Figs. 3(e) and 3(f) for the cases of $\kappa = 10\alpha$ (with $N = 12$ cells) and $\kappa = \alpha$ (with $N = 25$ cells), respectively. The (-3-dB) isolation bandwidth is roughly proportional to the strength of κ. For $\kappa = 10\alpha$ [Fig. 3(e)] the bandwidth is about 0.35%. Notably, even when $\kappa = \alpha$, i.e., when the quantized topological magnetoelectric polarizability has its minimum value, the transmission asymmetry can be quite strong and have a (-3-dB) bandwidth on the order of 0.05%, which, despite being rather modest in percentage, corresponds to 90 GHz in absolute value when the design wavelength is 1.55 μm. This value is large enough to easily accommodate typical optical communication links which usually have bandwidths in the range of few tens of gigahertz. It is also worth emphasizing that a magnetoelectric coupling with $\kappa = \alpha$ has a strength comparable to that characteristic of Cr_2O_3 [32]. Hence, the results of Fig. 3 show that media with a spontaneous nonreciprocal response may, indeed, be an interesting and promising route to implement a device that can be highly sensitive to the direction of the wave flow for circularly polarized light, especially if materials with a moderately large κ ($\sim 10\alpha$) are available.

B. Truncated magneto-optical photonic crystal

At optical frequencies the conventional solution to obtain an asymmetric electromagnetic response relies on iron garnets and takes advantage of the fact that these materials are nearly optically transparent [9–11]. Here, we explore the design of a nonreciprocal element with strongly asymmetric transmissions for circularly polarized waves based on the bismuth iron garnet (BIG). When biased with a static magnetic field oriented along the z direction, this material is modeled by the following constitutive relations [9]:

$$\mathbf{D} = \varepsilon_0 \bar{\varepsilon}_b \cdot \mathbf{E}, \qquad \mathbf{B} = \mu_0 \mu_b \mathbf{H}, \qquad (6)$$

where μ_b is the relative permeability and $\bar{\varepsilon}_b$ is the relative permittivity matrix,

$$\bar{\varepsilon}_b = \begin{pmatrix} \varepsilon_b & -i\kappa_b & 0 \\ i\kappa_b & \varepsilon_b & 0 \\ 0 & 0 & 1 \end{pmatrix}. \qquad (7)$$

As is well known, waves with polarization $\mathbf{e}_\pm$ [with an electric field of the form $\mathbf{E} = E(z)\mathbf{e}_\pm$] propagate in this magneto-optical material along the z direction in the same manner as in an isotropic dielectric with equivalent permittivity $\varepsilon_\pm = \varepsilon_b \pm \kappa_b$ and permeability μ_b. Thus, circularly polarized waves with different helicities experience different refractive indices and different wave impedances. As a consequence, the transmission coefficients for a layered structure [Fig. 4(a)] are generally different $T_+ \neq T_-$. Similar to the previous

(a)

(b)

(c)
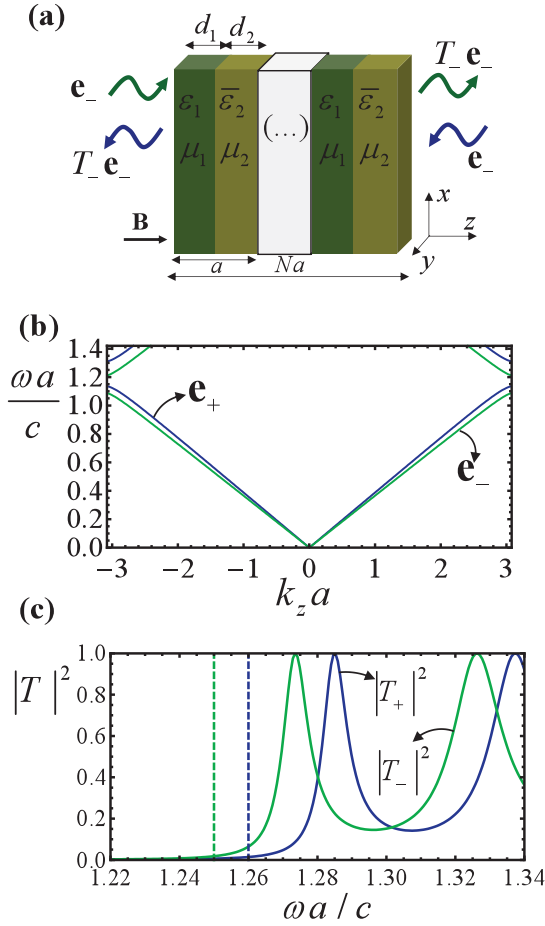
FIG. 4. Nonreciprocal element based on a bismuth iron garnet photonic crystal. (a) Truncated photonic crystal with a unit cell formed by a silicon slab and a bismuth iron garnet slab for the case of an extremely asymmetric transmission such that only waves with $\mathbf{e}_-$ polarization can be transmitted through the structure. (b) Band diagram of a photonic crystal with $d_1 = 0.15a$, $d_2 = 0.85a$, and $\kappa_b = -0.5$. (c) Transmissivities $|T_+|^2$ and $|T_-|^2$ as a function of the normalized frequency for a truncated structure with $N = 18$ cells and $\kappa_b = -0.06$. The green (blue) dashed vertical lines define the upper band-gap edges of the dispersion diagrams for $\mathbf{e}_-$ ($\mathbf{e}_+$).

subsection, the transmission coefficients are independent of the direction of the wave flow, and hence Eq. (5) also holds in the present case. On the other hand, the reflection coefficients are sensitive to the direction of arrival of the incoming wave and hence are denoted as $R_\pm^L, R_\pm^R$. The subscripts "$\pm$" determine the wave polarization and the superscripts "L, R" identify the direction of propagation of the incoming wave. The transmission and reflection coefficients $R_\pm^L, R_\pm^R$, and $T_\pm$ for the stratified structure are computed using standard methods, taking into account that the analysis can be reduced to a propagation problem in a structure with isotropic dielectrics.

Even though a single BIG layer would suffice to have $T_+ \neq T_-$, here we explore instead a photonic crystal design to enhance the asymmetric response which would otherwise be relatively weak. As a starting point, we compute the band diagram of a magneto-optical photonic crystal with a unit cell formed by a silicon layer ($\varepsilon_1 = 11.9$ and $\mu_1 = 1$)

and by a magnetized BIG slab. Following Ref. [9], for wavelengths near $\lambda_0 = 1.55\,\mu$m the BIG may be modeled by the parameters $\varepsilon_b = 6.25$ and $\kappa_b = -0.06$. The required bias field is estimated to be on the order of 0.04 T, and it is assumed that κ_b does not vary appreciably with the frequency in the range of interest [11]. The band diagram of the eigenstates with polarization $\mathbf{e}_\pm$ is obtained from the dispersion equation [42],

$$(T_\pm^L e^{-ik_z a} - 1)(T_\pm^R e^{ik_z a} - 1) - R_\pm^L R_\pm^R = 0, \qquad (8)$$

where k_z is the propagation constant along the periodic structure and the relevant reflection and transmission coefficients $(T_\pm^L, T_\pm^R, R_\pm^L, R_\pm^R)$ are calculated in a scenario wherein a single unit cell of the crystal stands alone in free space. The period of the unit cell is a, and the thicknesses of the two slabs are $d_1 = 0.15a$ and $d_2 = 0.85a$. These values were obtained after some optimization that targeted the band splitting of the $\mathbf{e}_\pm$ eigenstates.

The calculated band structure is represented in Fig. 4(b). In this simulation we used $\kappa_b = -0.5$ (rather than the realistic value $\kappa_b = -0.06$) so that the difference between the two polarizations is evident in the scale of the plot. As seen, near the band-gap edges the dispersion of the two modes can differ significantly. In particular, around $\omega a/c \approx 1.27$ (near the upper band-gap edge), the only propagating mode is associated with the $\mathbf{e}_-$ eigenstate. This discrimination between the two eigenmodes $\mathbf{e}_\pm$ creates the opportunity for strongly asymmetric transmissions in a truncated photonic crystal. This is illustrated in Fig. 4(c) for the realistic material parameters $\varepsilon_b = 6.25$ and $\kappa_b = -0.06$. Specifically, Fig. 4(c) depicts the transmissivities $|T_+|^2$ and $|T_-|^2$ as a function of the normalized frequency $\omega a/c$ for the case of a layered structure with $N = 18$ unit cells. Importantly, for $\omega a/c \approx 1.27$ the coefficient $|T_+|^2$ is near zero, whereas $|T_-|^2$ is approximately unity. In a design for which the peak of transmission ($\omega a/c \approx 1.27$) corresponds to $\lambda_0 = 1.55\,\mu$m the period of the unit cell is $a = 313$ nm.

It is interesting to note that the bandwidth (0.78%) and the discrimination between $|T_+|^2$ and $|T_-|^2$ provided by the BIG nonreciprocal element (which requires a biasing field) are comparable with what is achieved with an electronic topological insulator with $\kappa \approx \kappa_b$ [compare Figs. 4(c) and 3(e)]. This further underlines that media with a spontaneous magnetoelectric response may determine an exciting solution for optical isolation. However, the condition $\kappa \approx \kappa_b$ requires a magnetoelectric (Tellegen) parameter on the order of 10α. Consistent with this observation, the bandwidth obtained with the BIG nonreciprocal device is substantially better (one order of magnitude) than the bandwidth obtained an electronic topological insulator with the minimal quantized topological magnetoelectric polarizability [$\kappa = \alpha$; see Fig. 3(f)].

C. Ferrite slab

For completeness, we also discuss the possibility of a ferrite-based nonreciprocal element, which can be interesting for microwave applications. Indeed, at microwave frequencies, ferrites are the preferred solution to obtain a strong nonreciprocal response [5]. A ferrite biased with a static magnetic field oriented along the z axis is characterized by

the constitutive relations,

$$\mathbf{D} = \varepsilon_0 \varepsilon_f \mathbf{E}, \qquad \mathbf{B} = \mu_0 \bar{\mu}_f \cdot \mathbf{H}, \qquad (9)$$

where ε_f is the relative permittivity and $\bar{\mu}_f$ is the relative permeability matrix given by

$$\bar{\mu}_f = \begin{pmatrix} \mu_f & -i\kappa_f & 0 \\ i\kappa_f & \mu_f & 0 \\ 0 & 0 & 1 \end{pmatrix}. \qquad (10)$$

The parameters μ_f and κ_f depend on the frequency as

$$\mu_f = 1 + \frac{(\omega_0 - i\alpha_f \omega)\omega_m}{(\omega_0 - i\alpha_f \omega)^2 - \omega^2}, \qquad \kappa_f = \frac{\omega \omega_m}{(\omega_0 - i\alpha_f \omega)^2 - \omega^2}, \qquad (11)$$

where $\omega_0 = \mu_0 \gamma_R H_0$ is the precession or Larmor frequency determined by the bias magnetic field H_0 and by the gyromagnetic ratio γ_R, $\omega_m = \mu_0 \gamma_R M_s$ is the Larmor frequency for the saturation magnetization M_s, and α_f is a (dimensionless) damping factor [5].

Interestingly, the response of a ferrite is qualitatively similar to that of the magneto-optical material studied in the previous subsection. In particular, the eigenstates of the scattering problem [for the geometry of Fig. 5(a)] are also $\mathbf{e}_\pm$, and

(a)

(b)

(c)
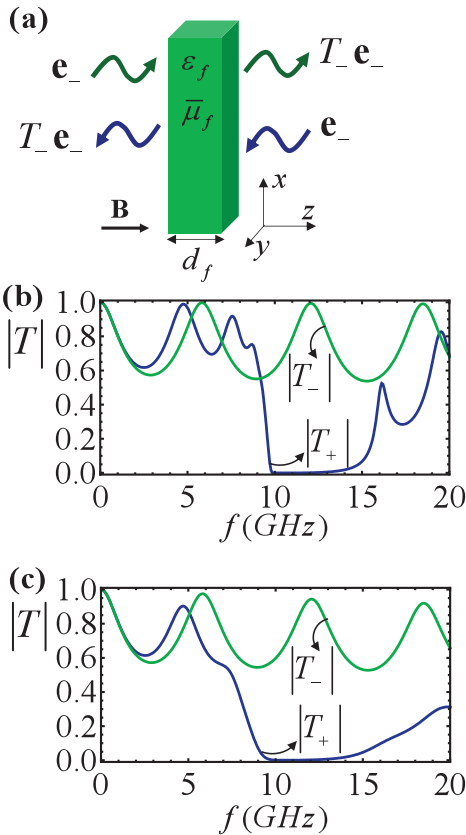
FIG. 5. Nonreciprocal element formed by a ferrite slab. (a) Scattering of a circularly polarized plane wave by a ferrite slab in air for the case of an extremely asymmetric transmission. In the regime of interest, only waves associated with the $\mathbf{e}_-$ eigenstate can be transmitted through the structure. (b) and (c) Transmission coefficients $|T_+|$ and $|T_-|$ as a function of the frequency for different values of the damping factor α_f. (b) $\alpha_f = 10^{-2}$. (c) $\alpha_f = 10^{-1}$.

the corresponding transmission coefficients satisfy Eq. (5). Moreover, circularly polarized waves associated with the vector $\mathbf{e}_\pm$ propagate in the ferrite (along the z direction) as in an isotropic material with permittivity ε_f and permeability $\mu_\pm = \mu_f \pm \kappa_f$ given by $\mu_\pm = 1 + \frac{\omega_m}{\omega_0 \mp \omega - \omega i \alpha_f}$. Importantly, because the strength of the nonreciprocal effects at microwaves can be much larger than at optical frequencies (particularly, when the Larmor frequency is tuned to be near the spectral range of interest), it is possible to achieve strongly asymmetric transmissions with a *single* ferrite slab. The transmission coefficients for a ferrite slab with thickness d_f are given by

$$T_\pm^L = T_\pm^R$$

$$\equiv T_\pm = \frac{2\eta_0 \eta_\pm}{2\eta_0 \eta_\pm \cos(\beta_\pm d_f) - i(\eta_0^2 + \eta_\pm^2)\sin(\beta_\pm d_f)}, \qquad (12)$$

where the longitudinal wave numbers satisfy $\beta_\pm = k_0 n_\pm$ with $n_\pm = \sqrt{\varepsilon_f \mu_\pm}$ being the refractive indices of the equivalent isotropic media and $\eta_\pm = \eta_0 \sqrt{\mu_\pm / \varepsilon_f}$ being the corresponding wave impedances.

It is relatively simple to create highly asymmetric transmissions above the ferrimagnetic resonance, i.e., when $\omega > |\omega_0|$. For example, if the biasing field is along the $+z$ direction the Larmor frequency is positive, $\omega_0 > 0$, and hence for $\omega_0 < \omega < \omega_0 + \omega_m$, one has $\mu_+ < 0$ so that the ferrite is opaque to waves with the $\mathbf{e}_+$ polarization, leading to $|T_+| \to 0$ for a sufficiently thick slab. Thus, the propagation of waves associated with the $\mathbf{e}_+$ eigenstate can be nearly suppressed in the spectral range of $\omega_0 < \omega < \omega_0 + \omega_m$. On the other hand, the ferrite remains transparent to waves associated with the $\mathbf{e}_-$ eigenstate ($\mu_- > 1$). Hence, if the material loss is small, it is possible to ensure that the waves with the $\mathbf{e}_-$ helicity are tunneled through the ferrite slab with $|T_-| \approx 1$ by tuning the slab thickness in such a manner that $d_f = m\pi/\beta_-$, $m = 1, 2, \ldots$ (mth Fabry-Pérot resonance) at the desired frequency of operation. Usually, the frequency of operation should be chosen in the middle of the gap $\omega \sim \omega_0 + \omega_m/2$ because this provides a more robust operation in the presence of loss and a better discrimination between the responses of the two eigenstates $\mathbf{e}_\pm$.

To illustrate these ideas, we depict in Figs. 5(b) and 5(c) the transmission coefficient for each eigenstate $|T_+|$ and $|T_-|$ as a function of the frequency for two realistic values of the damping factor α_f [5]. In these simulations, it is assumed that the ferrite is characterized by $\varepsilon_f = 14 + i0.001$, $\omega_0/2\pi = 10\,\text{GHz}$, and $\omega_m/2\pi = 5.04\,\text{GHz}$. These values correspond to a biasing magnetic field of $B_0 = 0.357\,\text{T}$ and to a saturation magnetization of $\mu_0 M_s = 0.18\,\text{T}$, which are typical values for microwave ferrites [5]. The frequency of operation is chosen as $1.2\omega_0$ (12 GHz) and the thickness of the slab was tuned to satisfy $d_f = 2\pi/\beta_- = 6\,\text{mm}$ (second-order Fabry-Pérot resonance at 12 GHz). As seen in Fig. 5, around the design frequency, there is a nearly perfect and wideband discrimination between the two relevant eigenstates such that $|T_-| \approx 1$ and $|T_+| \approx 0$ at 12 GHz, even in the presence of significant material loss. This robustness is made possible by the strong magnetic anisotropy of ferrites at microwave wavelengths and contrasts with the comparably much weaker

nonreciprocal response of magneto-optical materials in the optical regime.

V. DISCUSSION AND EXAMPLES

In the following, we illustrate how by combining the responses of a nonreciprocal element with a strongly asymmetric transmissivity response (e.g., a topological insulator photonic crystal) and a chiral metamaterial with a large circular dichroism it may be possible to have a nearly ideal optical isolation of circularly polarized light.

To begin with, it is useful to note—with respect to the general configuration of Fig. 1(a)—that the global transmission coefficients $T_\pm^{R,L}$ are generally related to the transmission and reflection coefficients of each sub-block ($T_{\chi,\pm}^{R,L}$, $R_{\chi,\pm}^{R,L}$ for the chiral slab and $T_{\kappa,\pm}^{R,L}$, $R_{\kappa,\pm}^{R,L}$ for the nonreciprocal element) as $T_\pm^L = \frac{T_{\kappa,\pm}^L T_{\chi,\pm}^L}{1-R_{\kappa,\pm}^R R_{\chi,\pm}^L}$ and $T_\pm^R = \frac{T_{\kappa,\pm}^R T_{\chi,\pm}^R}{1-R_{\kappa,\pm}^R R_{\chi,\pm}^L}$. Using the fact that the reflection coefficient of a chiral slab is independent of the polarization and of the direction of arrival of the incoming wave $R_{\chi,\pm}^L = R_{\chi,\pm}^R \equiv R_\chi$ that $T_{\chi,\pm}^R = T_{\chi,\mp}^L$ and that for all configurations of interest $T_{\kappa,\pm}^L = T_{\kappa,\pm}^R \equiv T_{\kappa,\pm}$, it is also possible to write

$$T_\pm^L = \frac{T_{\kappa,\pm} T_{\chi,\pm}^L}{1-R_{\kappa,\pm}^R R_\chi}, \qquad T_\pm^R = \frac{T_{\kappa,\pm} T_{\chi,\mp}^L}{1-R_{\kappa,\pm}^R R_\chi}. \qquad (13)$$

In the ideal regime of optical isolation, the reflection coefficient of the chiral slab vanishes $R_\chi = 0$, and hence in these conditions one obtains $T_\pm^L = T_{\kappa,\pm} T_{\chi,\pm}^L$ and $T_\pm^R = T_{\kappa,\pm} T_{\chi,\mp}^L$. Thus, it follows that if the regimes of strongly asymmetric transmissions considered in Secs. III and IV are combined only one of the four coefficients $T_\pm^L$ and $T_\pm^R$ has amplitude near the unity, whereas the remaining three coefficients are near zero. This rigorous analytical result complements the semiheuristic arguments given in Sec. II and confirms that in ideal conditions the combination of the two sub-blocks can give, indeed, a perfect optical isolation.

A. Truncated Tellegen-type photonic crystal and chiral metamaterial

In the first design [Fig. 6(a)], we consider an isolator based on an optical chiral metamaterial and on a nonreciprocal element formed by a truncated topological insulator photonic crystal. The chiral metamaterial slab has the same structural parameters as in Fig. 2(b), and the truncated photonic crystal has the same geometry as in Fig. 3.

In the first example, we consider a photonic crystal with $\kappa = 10\alpha$ and $N = 12$ cells. The lattice constant is taken equal to $a = 545$ nm to have an asymmetric response that overlaps the asymmetric response of the chiral metamaterial of Fig. 2(b). Figure 6(b) shows the different transmissivities versus frequency for the proposed optical isolator. As seen, near 188.5 (THz) we have $|T_-^L|^2 \approx 1$, whereas the remaining transmissivities are near zero. The bandwidth of operation is about 0.28% and corresponds roughly to the individual bandwidth of the nonreciprocal element. In particular, the RCP polarized waves are completely blocked by the optical isolator ($|T_+^L|^2 \approx 0 \approx |T_-^R|^2$), whereas the transmission of
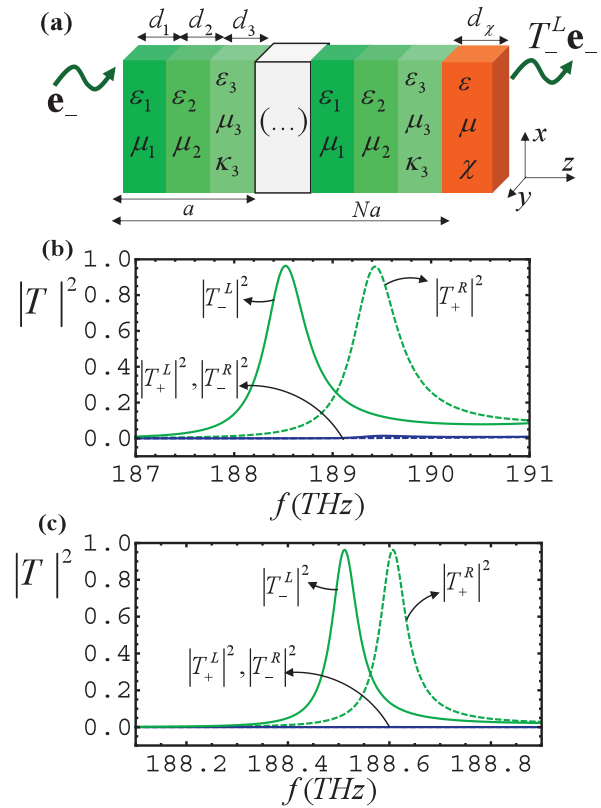
FIG. 6. Optical isolator formed by a truncated Tellegen photonic crystal and a chiral metamaterial. (a) Geometry of the optical isolator. In the ideal regime, the wave transmission is only possible from the left to the right and for LCP waves. (b) Transmissivities as a function of the frequency for a Tellegen parameter $\kappa = 10\alpha$. (c) Similar to (b) but for the Tellegen parameter $\kappa = \alpha$.

LCP polarized waves from right to left is also strongly suppressed $|T_+^R|^2 \approx 0.03$ at the design frequency. Thus, only LCP waves propagating in the direction left to right are effectively transmitted through the system. A better discrimination between $|T_+^R|^2$ and $|T_+^L|^2$ may be obtained by considering a nonreciprocal element with a larger number of cells and hence with a larger thickness.

In the second example [Fig. 6(c)], we studied the response of an optical isolator formed by a photonic crystal with 25 cells and a minimal value of the quantized magnetoelectric polarizability ($\kappa = \alpha$). As seen, the response is qualitatively similar to that of the first example, but due to the weaker magnetoelectric polarizability the bandwidth is narrower (0.033%). As previously mentioned, the bandwidth is roughly proportional to the Tellegen parameter. In this case we have $|T_+^R|^2/|T_-^L|^2 \approx 0.04$ at the design frequency.

B. Truncated magneto-optical photonic crystal and chiral metamaterial

In the second design, the nonreciprocal element is a truncated photonic crystal with a unit cell formed by silicon and magnetized bismuth iron garnet slabs, similar to the geometry of Sec. IV B. The truncated photonic crystal is juxtaposed to the same chiral metamaterial as in the previous
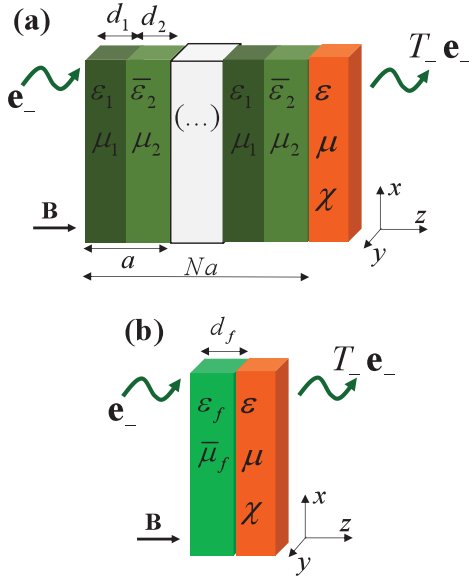
FIG. 7. Two designs for an electromagnetic isolator. In the regime of interest, only LCP waves propagating from the left to the right can go through the isolator. (a) A bismuth iron garnet photonic crystal juxtaposed to a chiral metamaterial. (b) A ferrite slab juxtaposed to a chiral metamaterial.

subsection [Fig. 7(a)], and the period of the unit cell of the photonic crystal is chosen equal to $a = 322.5$ nm so that the asymmetries of the two elements occur at the same frequency. The calculated transmissivities for circularly polarized waves as a function of frequency are represented in Fig. 8(a). As in the example of Fig. 4(c), the truncated photonic crystal is formed by $N = 18$ cells, $d_1 = 0.15a$ and $d_2 = 0.85a$.
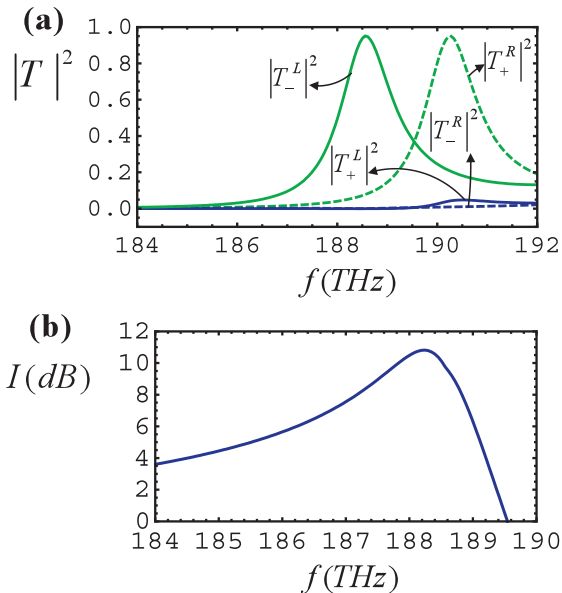
FIG. 8. Optical isolator formed by a truncated bismuth iron garnet photonic crystal and a chiral metamaterial. (a) Transmissivities as a function of frequency. (b) Isolation in decibels as a function of frequency.
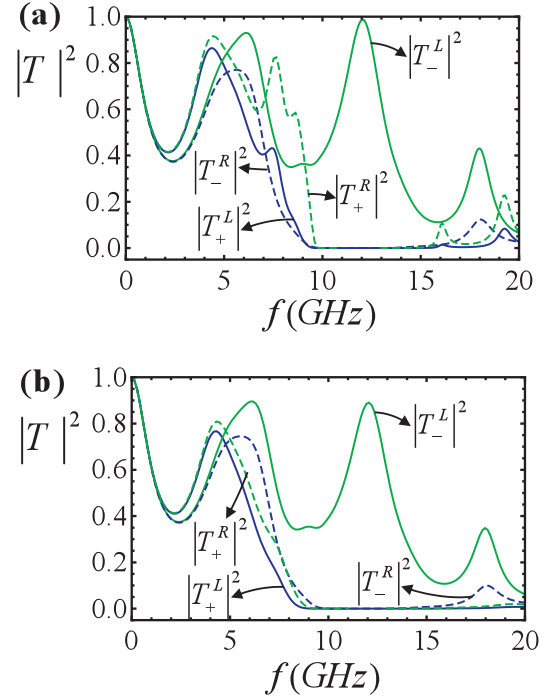
FIG. 9. Electromagnetic isolator formed by a ferrite slab and a chiral metamaterial. (a) and (b) Transmission coefficients as a function of the frequency for the ferrite damping factor (a) $\alpha_f = 10^{-2}$ and (b) $\alpha_f = 10^{-1}$.

The results of Fig. 8(a) are qualitatively similar to those reported in the previous subsection for a nonreciprocal element with a spontaneous nonreciprocal response. In particular, at a frequency of 188.4 THz there is a quite robust optical isolation between the two air semispaces such that only LCP waves can propagate from the left to the right ($|T_-^L|^2 = 97\%$). Comparing Fig. 8(a) with Fig. 6(b)—which refer to nonreciprocal elements with $\kappa \sim \kappa_b$—it is seen that the bandwidth is slightly better in the present example (0.71%). Figure 8 depicts the isolation $I = 10 \log_{10}(|T_-^L|^2/|T_+^R|^2)$ as a function of frequency. As seen, the isolation peak is on the order of $I \approx 11$ dB, which is a good result considering that the proposed structure is quite compact.

C. Ferrite slab and chiral metamaterial

In the final example, we consider the design of an electromagnetic isolator for microwaves. The isolator is formed by a ferrite slab juxtaposed to a chiral metamaterial as shown in Fig. 7(b). The parameters of the ferrite slab are the same as in the example of Sec. IV C. For simplicity, the microwave chiral medium is modeled with the Condon model [Eq. (1)], but in practice it can be implemented relying on structured metamaterials similar to the optical design reported in Sec. III [44,50]. The parameters of the Condon model are as in the example of Fig. 2(a) with ω_{R0} tuned so that 12 GHz is the frequency wherein the circular dichroism is maximal. The chiral slab thickness is $d = 8$ mm.

Figures 9(a) and 9(b) depict the transmissivities of the proposed microwave isolator as a function of frequency for typical values of the ferrite damping factor. As seen, consistent with the discussion of Sec. II, when the nonreciprocal element

is combined with the chiral slab, the resulting structure behaves as a nearly ideal electromagnetic diode around the design frequency (12 GHz) for completely realistic values of the ferrite loss. Due to the strong anisotropic nonreciprocal response of the ferrite near the ferrimagnetic resonance, this design is very wideband, and the wave propagation is only allowed from the left to the right and for LCP waves.

VI. CONCLUSION

We proposed a different paradigm for optical isolation of circularly polarized light based on the combination of a nonreciprocal element and a chiral metamaterial. It was theoretically shown that in ideal circumstances, such a solution may ensure a nearly perfect isolation between two regions of space such that the wave propagation may be unidirectional and only allowed for light states with a very specific helicity. Three different solutions for the nonreciprocal element were considered: (i) a truncated photonic crystal formed by materials with a spontaneous nonreciprocal response, (ii) a truncated photonic crystal formed by a magnetized magneto-optical material, and (iii) a magnetized ferrite slab. Due to the weak nonreciprocal response of natural materials at optical frequencies, the bandwidths of the proposed optical designs are relatively small in percentage but sufficiently large in absolute value (typically exceeding 100 GHz) to easily accommodate the bandwidths of conventional optical links. Some of the proposed designs may be challenging to realize in practice due to the fact that the nonreciprocal element is formed by many alternating layers of different materials. However, the current state of the art of nanofabrication techniques enables the fabrication of structures with as many as 20 stacked layers [53], and hence it seems that the realization of our structures may be within reach. We numerically verified that the proposed designs are robust to random perturbations in the thickness of the material layers on the order of 2%. Larger perturbations (up to 10%) lead to small shifts in the operation frequency but do not affect the split of the responses to circularly polarized waves with different helicities.

Solution (i) is especially interesting because it does not require a biasing field. Moreover, it was suggested that this solution can be implemented relying on a spontaneous topological magnetoelectric effect in antiferromagnetic topological insulators. It was demonstrated that the nonreciprocal magnetoelectric response can be strongly enhanced in a photonic crystal near the band-gap edges due to Bragg diffraction effects. Notably, even for the minimal quantized value of the magnetoelectric polarizability, the response of the nonreciprocal element can be sufficiently strong to allow for a strong discrimination of the two circularly polarized light states. However, in order that solution (i) can be competitive with typical optical designs the magnetoelectric coupling parameter is required to be on the order of $\kappa \sim 10\alpha$, which in practice may be challenging to obtain. If this obstacle can be overcome, media with a spontaneous nonreciprocal response can have really exciting applications in optical isolation and in unidirectional propagation.

ACKNOWLEDGMENTS

[1] D. Jalas, A. Petrov, M. Eich, W. Freude, S. Fan, Z. Yu, R. Baets, M. Popović, A. Melloni, J. D. Joannopoulos, M. Vanwolleghem, C. R. Doerr, and H. Renner, What is — and what is not — an optical isolator, Nat. Photonics **7**, 579 (2013).

[2] A. Figotin and I. Vitebsky, Nonreciprocal magnetic photonic crystals, Phys. Rev. E **63**, 066609 (2001).

[3] A. Figotin and I. Vitebskiy, Frozen light in photonic crystals with degenerate band edge, Phys. Rev. E **74**, 066613 (2006).

[4] P. Yeh, *Optical Waves in Layered Media* (Wiley, Hoboken, NJ, 1998).

[5] D. M. Pozar, *Microwave Engineering* (Addison Wesley, Reading, MA, 1990).

[6] T. Kodera and C. Caloz, Uniform ferrite-loaded open waveguide structure with CRLH response and its application to a novel backfire-to-endfire leaky-wave antenna, IEEE Trans. Microwave Theory Tech. **57**, 784 (2009).

[7] A. Parsa, T. Kodera, and C. Caloz, Ferrite based non-reciprocal radome, generalized scattering matrix analysis and experimental demonstration, IEEE Trans. Antennas Propag. **59**, 810 (2011).

[8] T. Kodera, D. L. Sounas, and C. Caloz, Magnetless nonreciprocal metamaterial (MNM) technology: Application to microwave components, IEEE Trans. Microw. Theory Techn. **61**, 1030 (2013).

[9] K. Fang, Z. Yu, V. Liu, and S. Fan, Ultracompact nonreciprocal optical isolator based on guided resonance in a magneto-optical photonic crystal slab, Opt. Lett. **36**, 4254 (2011).

[10] N. Adachi, V. P. Denysenkov, S. I. Khartsev, and A. M. Grishin, Epitaxial $Bi_3Fe_5O_{12}$(001) films grown by pulsed laser deposition and reactive ion beam sputtering techniques, J. Appl. Phys. **88**, 2734 (2000).

[11] T. Tepper and C. A. Ross, Pulsed laser deposition and refractive index measurement of fully substituted bismuth iron garnet films, J. Cryst. Growth **255**, 324 (2003).

[12] A. R. Davoyan and N. Engheta, Theory of Wave Propagation in Magnetized Near-Zero-Epsilon Metamaterials: Evidence for One-Way Photonic States and Magnetically Switched Transparency and Opacity, Phys. Rev. Lett. **111**, 257401 (2013).

[13] V. Temnov, G. Armelles, U. Woggon, D. Guzatov, A. Cebollada, A. Garcia-Martin, J. M. Garcia-Martin, T. Thomays, A. Leitenstorfers, and R. Bratschitschs, Active magneto-plasmonics in hybrid metal–ferromagnet structures, Nat. Photonics **4**, 107 (2010).

[14] V. I. Belotelov, L. L. Doskolovich, and A. K. Zvezdin, Extraordinary Magneto-Optical Effects and Transmission through Metal-Dielectric Plasmonic Systems, Phys. Rev. Lett. **98**, 077401 (2007).

[15] J. Y. Chin, T. Steinle, T. Wehlus, D. Dregely, T. Weiss, V. I. Belotelov, B. Stritzker, and H. Giessen, Nonreciprocal plasmonics enables giant enhancement of thin-film Faraday rotation, Nat. Commun. **4**, 1599 (2013).

[16] Z. Yu, Z. Wang, and S. Fan, One-way total reflection with one-dimensional magneto-optical photonic crystals, Appl. Phys. Lett. **90**, 121133 (2007).

[17] K. Gallo and G. Assanto, All-optical diode based on second-harmonic generation in an asymmetric waveguide, J. Opt. Soc. Am. B **16**, 267 (1999).

[18] A. E. Miroshnichenko, E. Brasselet, and Y. S. Kivshar, Reversible optical nonreciprocity in periodic structures with liquid crystals, Appl. Phys. Lett. **96**, 063302 (2010).

[19] Y. Ra'di, V. S. Asadchy, and S. A. Tretyakov, One-way transparent sheets, Phys. Rev. B **89**, 075109 (2014).

[20] T. Kodera, D. L. Sounas, and C. Caloz, Artificial Faraday rotation using a ring metamaterial structure without static magnetic field, Appl. Phys. Lett. **99**, 031114 (2011).

[21] D. L. Sounas, T. Kodera, and C. Caloz, Electromagnetic modeling of a magnetless and nonreciprocal gyrotropic metasurface, IEEE Trans. Antennas Propag. **61**, 221 (2013).

[22] A. M. Mahmoud, A. R. Davoyan, and N. Engheta, All-passive nonreciprocal metastructure, Nat. Commun. **6**, 8359 (2015).

[23] Z. Yu and S. Fan, Complete optical isolation created by indirect interband photonic transitions, Nat. Photonics **3**, 91 (2009).

[24] R. Fleury, D. L. Sounas, C. F. Sieck, M. R. Haberman, and A. Alù, Sound isolation and giant linear nonreciprocity in a compact acoustic circulator, Science **343**, 516 (2014).

[25] F. D. M. Haldane and S. Raghu, Possible Realization of Directional Optical Waveguides in Photonic Crystals with Broken Time-Reversal Symmetry, Phys. Rev. Lett. **100**, 013904 (2008).

[26] Z. Wang, Y. Chong, J. D. Joannopoulos, and M. Soljačić, Observation of unidirectional backscattering immune topological electromagnetic states, Nature (London) **461**, 772 (2009).

[27] L. Lu, J. D. Joannopoulos, and M. Soljačić, Topological photonics, Nat. Photonics **8**, 821 (2014).

[28] A. B. Khanikaev, S. H. Mousavi, W.-K. Tse, M. Kargarian, A. H. MacDonald, and G. Shvets, Photonic topological insulators, Nature Mater. **12**, 233 (2013).

[29] M. C. Rechtsman, J. M. Zeuner, Y. Plotnik, Y. Lumer, D. Podolsky, F. Dreisow, S. Nolte, M. Segev, and A. Szameit, Photonic Floquet topological insulators, Nature (London) **496**, 196 (2013).

[30] M. G. Silveirinha, Chern invariants for continuous media, Phys. Rev. B **92**, 125153 (2015).

[31] M. G. Silveirinha, Z_2 topological index for continuous photonic media, Phys. Rev. B **93**, 075110 (2016).

[32] D. N. Astrov, Magnetoelectric effect in chromium oxide, Sov. Phys. JETP **13**, 729 (1961).

[33] S. Coh and D. Vanderbilt, Canonical magnetic insulators with isotropic magnetoelectric coupling, Phys. Rev. B **88**, 121106 (2013).

[34] R. S. K. Mong, A. M. Essin, and J. E. Moore, Antiferromagnetic topological insulators, Phys. Rev. B **81**, 245209 (2010).

[35] X. L. Qi, R. Li, J. Zang, and S. C. Zhang, Inducing a magnetic monopole with topological surface states, Science **323**, 1184 (2009).

[36] F. Liu, J. Xu, and Y. Yang, Polarization conversion of reflected electromagnetic wave from topological insulator, J. Opt. Soc. Am. B **31**, 735 (2014).

[37] F. R. Prudêncio, S. A. Matos, and C. R. Paiva, A geometrical approach of duality transformations for tellegen media, IEEE Trans. Microwave Theory Tech. **62**, 1417 (2014).

[38] I. V. Lindell, A. H. Sihvola, S. A. Tretyakov, and A. J. Viitanen, *Electromagnetic Waves in Chiral and Bi-Isotropic Media* (Artech House, Boston, 1994).

[39] M. G. Silveirinha and S. I. Maslovski, Comment on Repulsive Casimir Force in Chiral Metamaterials, Phys. Rev. Lett. **105**, 189301 (2010).

[40] X. L. Qi and S. C. Zhang, Topological insulators and superconductors, Rev. Mod. Phys. **83**, 1057 (2011).

[41] A. G. Grushin and A. Cortijo, Tunable Casimir Repulsion with Three-Dimensional Topological Insulators, Phys. Rev. Lett. **106**, 020403 (2011).

[42] F. R. Prudêncio, S. A. Matos, and C. R. Paiva, Asymmetric band diagrams in photonic crystals with a spontaneous nonreciprocal response, Phys. Rev. A **91**, 063821 (2015).

[43] M. G. Silveirinha, Design of linear-to-circular polarization transformers made of long densely packed metallic helices, IEEE Trans. Antennas and Propag. **56**, 390 (2008).

[44] D. E. Fernandes and M. G. Silveirinha, Tractor beam with chiral light, Phys. Rev. A **91**, 061801 (2015).

[45] V. A. Fedotov, P. L. Mladyonov, S. L. Prosvirnin, A. V. Rogacheva, Y. Chen, and N. I. Zheludev, Asymmetric Propagation of Electromagnetic Waves Through a Planar Chiral Structure, Phys. Rev. Lett. **97**, 167401 (2006).

[46] R. Singh, E. Plum, C. Menzel, C. Rockstuhl, A. K. Azad, R. A. Cheville, F. Lederer, W. Zhang, and N. I. Zheludev, Terahertz metamaterial with asymmetric transmission, Phys. Rev. B **80**, 153104 (2009).

[47] C. Menzel, C. Helgert, C. Rockstuhl, E.-B. Kley, A. Tünnermann, T. Pertsch, and F. Lederer, Asymmetric Transmission of Linearly Polarized Light at Optical Metamaterials, Phys. Rev. Lett. **104**, 253902 (2010).

[48] R. Zhao, T. Koschny, E. N. Economou, and C. M. Soukoulis, Comparison of chiral metamaterial designs for repulsive Casimir force, Phys. Rev. B **81**, 235126 (2010).

[49] R. Zhao, L. Zhang, J. Zhou, T. Koschny, and C. M. Soukoulis, Conjugated gammadion chiral metamaterial with uniaxial optical activity and negative refractive index, Phys. Rev. B **83**, 035105 (2011).

[50] R. Zhao, T. Koschny, and C. M. Soukoulis, Chiral metamaterials: retrieval of the effective parameters with and without substrate, Opt. Express **18**, 14553 (2010).

[51] CST GmbH 2014 CST MICROWAVE STUDIO [http://www.cst.com].

[52] F. W. Hehl, Y. N. Obukhov, J. P. Rivera, and H. Schmid, Relativistic analysis of magnetoelectric crystals: Extracting a new 4-dimensional P odd and T odd pseudoscalar from Cr_2O_3 data, Phys. Lett. A **372**, 1141 (2008).

[53] J. Valentine, S. Zhang, T. Zentgraf, E. Ulin-Avila, D. A. Genov, G. Bartal, and X. Zhang, Three-dimensional optical metamaterial with a negative refractive index, Nature (London) **455**, 376 (2008).